# mpcGear: Multi-Point Conjugation Gear Mechanisms

KE CHEN, University of Science and Technology of China, China and Singapore University of Technology and Design, Singapore
JOSHUA JOHN SHI KAI LEE, Singapore University of Technology and Design, Singapore
JIANMIN ZHENG, Nanyang Technological University, Singapore
LIGANG LIU, University of Science and Technology of China, China and Laoshan Laboratory, China
PENG SONG*, Singapore University of Technology and Design, Singapore

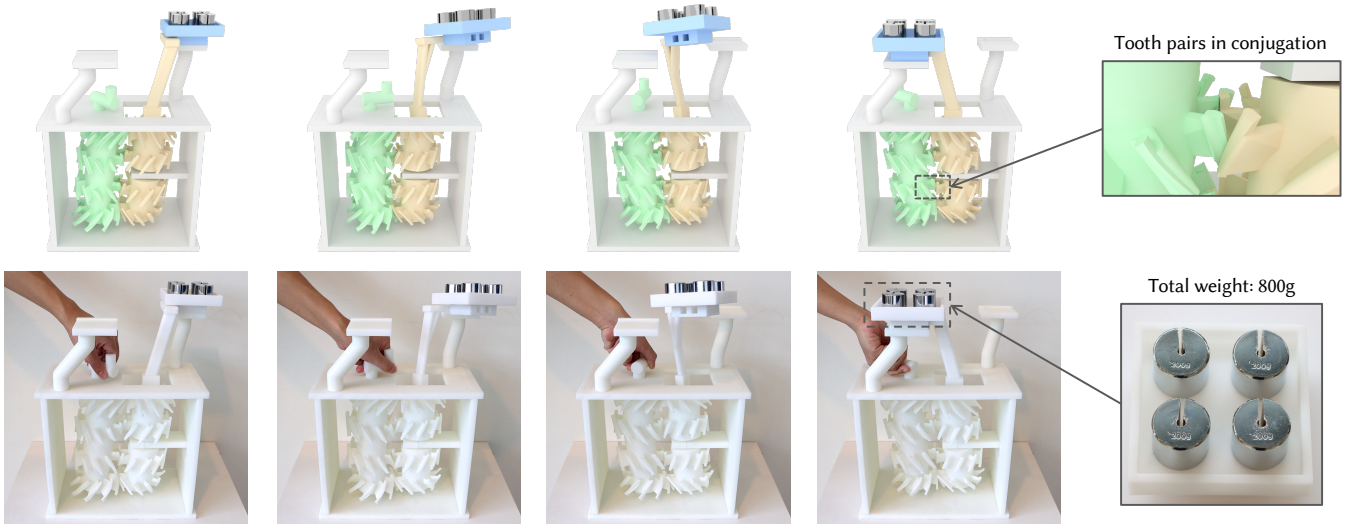


Fig. 1. We present a computational approach for modeling a new class of gear mechanisms called multi-point conjugation gear mechanisms that generate user-specified 3D motion under external loads. Using our approach, we model and fabricate a low-cost manipulator driven by a single actuator to perform a pick-and-place task while lifting a tray loaded with four 200g weights (totaling 800g).

Gears transmit rotary motion via meshing teeth, with circular gears commonly used to produce constant-speed rotation and non-circular gears enabling variable-speed rotation. In order to generate complex motion, gears are typically combined with other mechanical parts such as linkages, cam-followers, and belts, which often leads to complex structures and reduced transmission efficiency. To address these limitations, recent research has been investigating non-conventional gears that can transfer complex motion while preserving key properties of gears, such as compactness, high transmission efficiency, and load-bearing capability. In this paper, we present a new gear mechanism called the multi-point conjugation gear mechanism for exactly generating a user-specified 3D motion under external loads. The mechanism contains a single pair of gears modeled by a pair of conjugate surfaces with multiple conjugation points. We introduce an optimization-based approach that designs this new gear mechanism by modeling multiple sub-gear pairs that satisfy multi-point conjugation and fabricability requirements, whose load-bearing performance is quantified using a measure of dynamic form closure. We demonstrate the effectiveness of our approach by modeling various multi-point conjugation gear mechanisms that generate different kinds of motions, evaluating their kinematic performance and load-bearing performance using 3D printed prototypes, and presenting two application examples.

CCS Concepts: • **Computing methodologies** → *Shape modeling*.

**ACM Reference Format:**
Ke Chen, Joshua John Shi Kai Lee, Jianmin Zheng, Ligang Liu, and Peng Song. 2026. mpcGear: Multi-Point Conjugation Gear Mechanisms. In *Special Interest Group on Computer Graphics and Interactive Techniques Conference Conference Papers (SIGGRAPH Conference Papers '26), July 19–23, 2026, Los Angeles, CA, USA*. ACM, New York, NY, USA, 11 pages. https://doi.org/10.1145/3799902.3811089

*Corresponding author.

Authors' Contact Information: Ke Chen, University of Science and Technology of China, China and Singapore University of Technology and Design, Singapore, ckck@mail.ustc.edu.cn; Joshua John Shi Kai Lee, Singapore University of Technology and Design, Singapore, joshua_leeshikai@mymail.sutd.edu.sg; Jianmin Zheng, Nanyang Technological University, Singapore, asjmzheng@ntu.edu.sg; Ligang Liu, University of Science and Technology of China, China and Laoshan Laboratory, China, lgliu@ustc.edu.cn; Peng Song, Singapore University of Technology and Design, Singapore, peng_song@sutd.edu.sg.


*SIGGRAPH Conference Papers '26, Los Angeles, CA, USA*

ACM ISBN 979-8-4007-2554-8/2026/07
https://doi.org/10.1145/3799902.3811089

## 1 Introduction

Gears are fundamental mechanisms that mesh together via teeth and are used to transfer rotary motion from one shaft to another. The

most common type is the circular gear, widely used for transferring rotary motion with a constant velocity ratio, such as spur gears for parallel shafts and bevel gears for intersecting shafts. Generalizing gear shapes from circular to non-circular enables variable-speed transmission [Litvin et al. 2009]. To generate complex motion beyond simple axial rotation, gears typically need to be combined with other mechanical components such as linkages [Coros et al. 2013], cam-followers [Zhu et al. 2012], and belts [Ceylan et al. 2013]. However, these compound mechanisms often result in large volume, poor dynamic balance, complex structures, and reduced transmission efficiency, and are particularly sensitive to the accumulation of manufacturing and assembly errors.

To address the above limitations, researchers are investigating non-conventional gears capable of generating motion beyond axial rotation, including non-circular bevel gears that generate rotation and axial translation [Hou and Lin 2020; Hu et al. 2021], spherical gears that output 3-DOF rotational motion driven by 4 actuators [Abe et al. 2021], and puzzle gears in which a single gear drives the spatial motions of multiple mated gears [Matsumoto and Segerman 2023; van Deventer 2019]. These non-conventional gears extend the motion generation capabilities of traditional gears, while aiming to preserve key properties of gears such as compact layouts, high transmission efficiency, and load-bearing capability. With increased geometric complexity, these non-conventional gears are typically fabricated using additive manufacturing techniques.

Following prior research on non-conventional gears, this paper aims to generalize conventional gear mechanisms to *3D freeform gear mechanisms*, enhancing their motion transmission ability while preserving the inherent load-bearing capability of gears. This is motivated by practical applications, where mechanisms are usually required to generate complex motions while remaining functional under external loads. Recently, Chen et al. [2024] proposed a multi-point conjugation mechanism (mpcMech) that can generate a 3-DOF motion exactly by satisfying the dynamic form closure condition. Inspired by this work, our idea is to model a pair of conjugate surfaces with multiple conjugation points as the gear geometry, forming a *multi-point conjugation gear mechanism* (mpcGear). By satisfying the dynamic form closure condition, a mpcGear can also generate a complex motion from a single actuator. However, realizing such a mpcGear introduces two main challenges. First, it is non-trivial to model a pair of fabricable gear surfaces that maintain multiple conjugation points throughout the motion. Second, it remains unclear how to quantify the load-bearing characteristics of such mechanisms. To address these challenges, our work makes the following contributions:

- We extend the dynamic form closure theory by introducing a quantitative measure of dynamic form closure, which not only determines whether a mechanism with multi-point conjugation can ensure continuous motion transmission, but also enables evaluation of its load-bearing performance.
- We develop an optimization-based approach to model the geometry of a multi-point conjugation gear mechanism for exactly generating a user-specified motion in $N$-DOF motion space, $1 \leqslant N \leqslant 4$. The approach models multiple sub-gear pairs (each composed of multiple tooth pairs) satisfying multi-point conjugation, and geometry fabricability, whose load-bearing performance is quantified and guided by the measure.

To demonstrate the effectiveness of our approach, we model a variety of multi-point conjugation gear mechanisms that generate motions in different kinds of motion spaces, evaluate their kinematic and load-bearing performance through physical experiments using 3D printed prototypes, and present two application examples to show the practical value of the new mechanism.

## 2 Related Work

*Mechanism design.* Mechanism design aims to design the geometry of a mechanism that transfers an input motion to a user-specified output motion with desired kinematic characteristics, such as a target trajectory or a sequence of rigid-body poses. Many studies in the graphics community design mechanisms by combining conventional mechanical components of simple geometry, such as linkages, cams, pulleys, joints, and gears, for practical applications including walking machines [Bharaj et al. 2015; Mannhart et al. 2020], mechanical characters [Coros et al. 2013; Megaro et al. 2014; Thomaszewski et al. 2014], drawing machines [Liu and McCarthy 2017; Roussel et al. 2018; Takahashi and Okuno 2018], mechanical toys [Zhu et al. 2012], mechanical figures that mimic human motions [Ceylan et al. 2013], wind-up toys [Song et al. 2017], mechanical papercrafts [Oh et al. 2017], kinetic wire characters [Xu et al. 2018], multi-pose mechanical objects [Nishida et al. 2019], robotic characters [Maloisel et al. 2023], clock mechanisms [Commin et al. 2025], and conformable mechanisms [Li et al. 2025]. With advances in additive manufacturing, researchers are developing novel mechanisms composed of mechanical components with non-standard geometries to accomplish increasingly complex motion tasks, including 3D cam-follower mechanisms for exact 2D path generation [Cheng et al. 2021], 3D cam-linkage mechanisms for exact 3D path generation [Cheng et al. 2022], and multi-point conjugation mechanisms for exact 3D motion generation [Chen et al. 2024].

*Gear mechanism.* Conventional gear shapes have long been constrained by traditional manufacturing processes such as milling and broaching [Gupta et al. 2017]. With modern digital fabrication, particularly 3D printing, gears with non-standard geometry can now be fabricated accurately and efficiently. This has enabled a variety of non-conventional gear designs for previously unattainable motion transfer tasks, including variable-speed non-circular bevel gears [Lv et al. 2016; Zheng et al. 2016], oval non-circular bevel gears that generate axial translation and rotation [Hou and Lin 2020], curve-face gears for a spatial finite helical motion [Hu et al. 2021], a spherical gear mechanism in which the 3-DOF rotation of a cross spherical gear is driven by the respective 2-DOF rotation of two monopole gears [Abe et al. 2021], puzzle gears in which a 1-DOF rotation or translation of a single gear drives the spatial motions of multiple mated gears for recreational purposes [Matsumoto and Segerman 2023; van Deventer 2019]. In addition, Xu et al. [2020] proposed a computational method to model non-circular gears that resemble a pair of given shapes. While the above works focus on non-conventional gears with specific kinematics or shapes, we aim to generalize gear mechanisms toward multi-point conjugation, to advance their complex motion transmission ability. To the best of

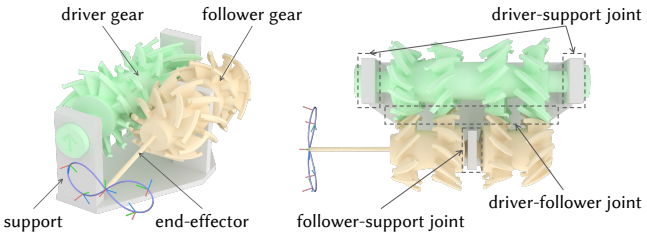


Fig. 2. A multi-point conjugation gear mechanism (mpcGear_3R) consists of a driver gear, a follower gear, a support, and the joints connecting them. An end-effector is attached to the follower gear to visualize the user-specified motion. Here, the follower-support joint is a spherical joint.

our knowledge, no existing gear mechanism consisting of a single gear pair driven by a single actuator is able to generate motions in motion space with more than 2 DOFs.

*Conjugate curves/surfaces.* The theory of conjugate curves or surfaces [Chen 1978] describes the necessary conditions for a pair of curves or surfaces to maintain continuous and tangent contact under a prescribed motion law. In the past decade, this theory has been widely applied to model gears with freeform tooth profiles and achieve improved mechanical properties, as the tooth curves or surfaces of a pair of mated planar or spatial gears are a pair of conjugate curves or surfaces [Wu and Luo 1992]. Notable developments based on conjugate curves and surfaces modeling include freeform conjugation theory and master-slave approach for 2D gears [Yu and Ting 2011, 2013a], extensions to spur and bevel gears by modeling 3D conjugate curves and deriving freeform or circular-arc tooth surfaces [Chen et al. 2014a,b; Yu and Ting 2013b], and helical gears with triple contact points modeled by three pairs of equidistant conjugate curves, which exhibit improved load capacity [Zhang et al. 2019]. While all the above gears are limited to transferring 1-DOF rotation to another 1-DOF rotation, Chen et al. [2024] recently proposed a multi-point conjugation mechanism that can transfer 1-DOF rotation to $N$-DOF motion ($1 \leqslant N \leqslant 3$) by modeling multiple conjugate curve pairs and satisfying the dynamic form closure condition. Building on this idea, our mpcGears satisfy the same condition and further aim to generate complex motions while preserving the load-bearing capability of gears.

## 3 Problem Formulation and Overview

Given a user-specified continuous periodic rigid-body motion in 3D space as input, our problem is to model a gear mechanism containing a single pair of gears that exactly generates this motion from a single actuator. This gear mechanism should satisfy:

(1) *Working mechanism.* The driver gear is able to drive the follower gear to perform the user-specified motion smoothly, continuously, and without collision.
(2) *Load-bearing mechanism.* Under external loads, the mechanism should keep the follower gear following the specified motion.
(3) *Fabricable mechanism.* The mechanism must be fabricable (e.g., via 3D printing), avoiding fragile features, particularly excessively thin gear teeth.

*Multi-point conjugation gear mechanisms.* We model the gear mechanism as a multi-point conjugation gear mechanism (mpcGear). A mpcGear consists of 3 mechanical parts: a *driver gear* performing a periodic 1-DOF rotation driven by a single actuator; a *follower gear* performing the user-specified motion driven by the driver gear; a *support* staying static to hold the gears; see Figure 2. The mechanism includes 3 mechanical joints: a *driver-support joint*, which is a revolute joint enabling the 1-DOF rotation of the driver gear; a *follower-support joint*, which determines the motion space of the follower gear (e.g., a spherical joint for the 3-DOF rotational motion space); a *driver-follower joint*, modeled as a multi-point conjugation joint that maintains multiple conjugation points between the driver gear and the follower gear during motion transmission. Modeling the driver-follower joint is the key to this mechanism.

*Classification of mpcGears.* mpcGears are classified according to the motion space determined by the follower-support joint. Each class is denoted as mpcGear_$N_R$R$N_T$T, where $N_R$ and $N_T$ represent the rotational and translational degrees of freedom (DOFs) of the motion space of the follower gear. For example, mpcGear_3R generates a motion in 3-DOF rotational motion space; see Figure 2. In this paper, we show four classes of mpcGears, categorized by the type of the follower-support joint: mpcGear_1R (revolute joint), mpcGear_1R1T (cylindrical joint), mpcGear_3R (spherical joint), and mpcGear_3R1T (moving spherical joint); see Figure 9.

*Overview of our approach.* Our task is to model a pair of conjugate surfaces with multiple conjugation points as the surfaces of the gear pair. To ensure a working mechanism, this surface pair should satisfy the dynamic form closure condition in [Chen et al. 2024]. Thus, Section 4.1 reviews the theory of conjugate surfaces with multi-point conjugation and the dynamic form closure condition. To evaluate the load-bearing performance, Section 4.2 introduces a measure of dynamic form closure, which also enables a reformulation of the original condition. Finally, Section 5 presents an optimization-based approach for modeling a working, load-bearing, and fabricable mpcGear.

## 4 Measure of Dynamic Form Closure

In our mpcGear, we model the geometry of the gears as a pair of conjugate surfaces with multiple conjugation points. In order to ensure continuous motion transmission, the conjugate surface pair should satisfy the dynamic form closure condition proposed in [Chen et al. 2024]. Section 4.1 reviews the relevant theoretical background from [Chen et al. 2024]. To evaluate the load-bearing performance of mechanisms with multiple conjugation points, Section 4.2 introduces a measure of dynamic form closure.

### 4.1 Background: Theory of mpcMech

In a mpcMech, the driver surface $\mathrm{S}^1$ and the follower surface $\mathrm{S}^2$ are modeled as a pair of conjugate surfaces with $K$ conjugation points. Under the dynamic form closure condition, the conjugate motion $\phi^1$ of $\mathrm{S}^1$ can drive the conjugate motion $\phi^2$ of $\mathrm{S}^2$ continuously.

*Multi-point conjugation.* Each conjugation point on the conjugate surface pair should satisfy the four conditions of single-point conjugation at any instant of motion: (1) *Coincide contact point.* The

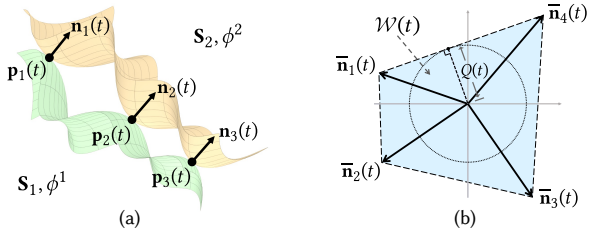


Fig. 3. (a) A pair of conjugate surfaces with 3 conjugation points at time $t$. The driver and follower surfaces are shown in green and yellow, respectively. (b) The measure of dynamic form closure $Q(t)$ is defined as the distance from $\mathbf{0}$ to the boundary of the attainable effective wrench set $\mathcal{W}(t)$.

two surfaces must coincide at the same contact point. (2) *Coincide contact normal.* At the contact point, their surface normals must be collinear but opposite in direction. (3) *Relative velocity.* The relative velocity must be perpendicular to the normal direction. (4) *Induced normal curvature.* The induced normal curvature along any tangential direction must be nonnegative. Please refer to [Chen et al. 2024] for their explicit expressions. Together, these four conditions ensure tangential contact at the conjugation point without immediate separation or interpenetration. The latter two conditions are automatically satisfied by our modeling approach. We denote the position and unit contact normal (pointing into the follower surface) of the $k$-th conjugation point at time $t$ by $\mathbf{p}_k(t)$ and $\mathbf{n}_k(t)$, respectively, $1 \leqslant k \leqslant K$; see Figure 3(a).

*Dynamic form closure condition.* Form closure is a classical concept in grasping for immobilizing rigid objects [Lakshminarayan 1978]. A set of frictionless contacts achieves (first-order) form closure if their positions and normals geometrically restrain any infinitesimal rigid motion of an object. In our setting, continuous motion transmission requires the driver surface to *dynamically form close* the follower surface throughout the motion. That is, at any time $t$, the multiple conjugation points restrain all infinitesimal rigid motions within the follower surface's motion space.

We represent an infinitesimal rigid motion by the nonzero generalized velocity $\mathbf{u} = [\mathbf{v}^\top, \boldsymbol{\omega}^\top]^\top \in \mathbb{R}^6$, where $\mathbf{v}$ and $\boldsymbol{\omega}$ are the linear and angular velocities, respectively. Without loss of generality, we restrict $\mathbf{u}$ to unit norm, i.e., $\|\mathbf{u}\| = 1$. We assume the driver surface and the follower surface perform periodic motions with period $T$ and maintain $K$ conjugation points at any time $t \in [0, T)$. The set of infinitesimal rigid motions of the follower surface restrained by the $k$-th conjugation point $\mathbf{p}_k(t)$ with normal $\mathbf{n}_k(t)$ at time $t$ is $U_k(t) = \{\, \mathbf{u} \mid \hat{\mathbf{n}}_k(t) \cdot \mathbf{u} < 0 \,\}$, where $\hat{\mathbf{n}}_k(t) = [\, \mathbf{n}_k(t)^\top, (\mathbf{p}_k(t) \times \mathbf{n}_k(t))^\top \,]^\top$ is the generalized normal. To achieve form closure on the follower surface for any $t \in [0, T)$, the $K$ conjugation points with normals $\{(\mathbf{p}_k(t), \mathbf{n}_k(t))\}$ should restrain all infinitesimal rigid motions of the follower surface, yielding the dynamic form closure condition:

$$U \subset \bigcup_{1 \leqslant k \leqslant K} U_k(t), \quad \forall\, t \in [0, T), \tag{1}$$

where $U$ is the infinitesimal $N$-DOF motion space of the follower surface, defined by the $N$-DOF follower-support joint as the set of all unit-norm infinitesimal rigid motions allowed by the joint. For example, when the user-specified motion is a 3-DOF rotation, the follower-support joint is chosen as a spherical joint. Thus $U = \{\, [\mathbf{0}, \boldsymbol{\omega}^\top]^\top \mid \|\boldsymbol{\omega}\| = 1 \,\}$, called a 3-DOF motion space. A necessary condition for Equation (1) is that the number of the conjugation points, $K$, satisfies

$$K \geqslant N + 1. \tag{2}$$

To exclude the degenerate case $U \bigcap U_k(t) = \emptyset$, we require:

$$\hat{\mathbf{n}}_k(t) \not\perp U, \quad \forall\, t \in [0, T),\ 1 \leqslant k \leqslant K. \tag{3}$$

## 4.2 Measure of Dynamic Form Closure

Under the dynamic form closure condition in Equation (1), the driver surface can continuously drive the follower surface to perform a motion. In practical applications, however, it is also important for the mechanism to maintain motion transmission while bearing external loads, such as payloads in robotic manipulation.

To quantify the load-bearing performance of a mechanism with multi-point conjugation that satisfies the dynamic form closure condition, we draw inspiration from [Cornellà and Suárez 2009]. Specifically, maintaining motion transmission under external loads requires the driver surface to counteract the components of external forces and torques that can induce rigid motions allowed by the follower-support joint, i.e., the components projected onto $\mathrm{span}(U)$, the linear space spanned by the motion space $U$. We therefore define an effective wrench as the wrench projected onto $\mathrm{span}(U)$. At time $t$, we define the measure as the worst-case attainable effective wrench magnitude over all motion directions in $U$: for each direction in $U$, we consider the maximum effective wrench magnitude in that direction, and then take the minimum over all directions. Equivalently, this measure is the distance from the zero vector $\mathbf{0}$ to the boundary of the attainable effective wrench set $\mathcal{W}(t)$; see Figure 3(b). Moreover, we show that $\mathcal{W}(t) = \mathrm{conv}(\, \{\overline{\mathbf{n}}_k(t)\}_{1 \leqslant k \leqslant K}\,)$, where $\mathrm{conv}(\cdot)$ is the convex hull operator and $\overline{\mathbf{n}}_k(t)$ is the projection of the generalized normal $\hat{\mathbf{n}}_k(t)$ onto $\mathrm{span}(U)$. Thus, the measure can be expressed as

$$Q(t) = -\,\mathrm{dist}(\mathbf{0}, \partial\, \mathrm{conv}(\, \{\overline{\mathbf{n}}_k(t)\}_{1 \leqslant k \leqslant K}\,)), \tag{4}$$

where $\mathrm{dist}(\cdot, \cdot)$ denotes the signed distance operator, taken as negative inside the convex hull, and $\partial$ denotes the boundary operator taken relative to $\mathrm{span}(U)$. The supplementary material provides a detailed derivation of $Q(t)$ for the above formulation and further shows that the dynamic form closure condition in Equation (1) is equivalent to $Q(t) > 0$ for all $t \in [0, T)$. We refer to $Q(t)$ as the *measure of dynamic form closure*. Overall, $Q(t) > 0$ guarantees continuous motion transmission, while a larger value of $Q(t)$ indicates better load-bearing performance of the mechanism.

# 5 Modeling Multi-Point Conjugation Gear Mechanisms

This section presents a bottom-up approach to modeling the geometry of a mpcGear, starting from a tooth pair (Section 5.1), a sub-gear pair (Section 5.2), multiple sub-gear pairs (Section 5.3), until a multi-point conjugation joint and a complete mechanism (Section 5.4).

The driver gear and the follower gear are modeled as a conjugate surface pair $\mathbf{S}^1$ and $\mathbf{S}^2$ with multi-point conjugation. Their respective conjugate motions, a periodic 1-DOF rotary motion $\phi^1$ and a

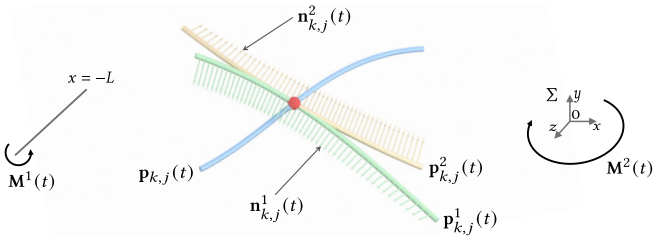


Fig. 4. Modeling a tooth pair, consisting of a pair of open 3D conjugate curves $\mathbf{p}^\alpha_{k,j}(t)$ with augmented normals $\mathbf{n}^\alpha_{k,j}(t)$, given the conjugate motion pair $\mathbf{M}^\alpha(t), \alpha \in \{1,2\}$. The blue curve denotes the locus curve $\mathbf{p}_{k,j}(t)$ and the red sphere denotes the conjugation point.

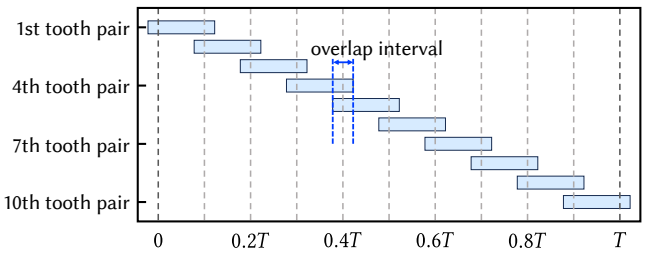


Fig. 5. Arrangement of the contact intervals for $J$ tooth pairs (illustrated using $J = 10$). Over the $j$-th subinterval $[(j-1)T/J,\ jT/J)$ of $[0,T)$, the $j$-th tooth pair maintains contact, $1 \leqslant j \leqslant J$.

user-specified 3D motion $\phi^2$, are expressed by homogeneous transformation matrices $\mathbf{M}^\alpha(t), \alpha \in \{1,2\}$, $t \in [0,T)$, in the fixed global frame $\Sigma(O-x,y,z)$. The origin $O$ is chosen as the follower-support joint center (e.g., the rotation center for rotational motions). The rotation axis of $\phi^1$ is fixed at $x = -L$ in the global frame $\Sigma$, where $L$ denotes the distance from the driver axis to the origin $O$, controlling the size of the mechanism. We fix $L = 25.0$ in our experiments. All geometric variables in this paper are defined in $\Sigma$.

## 5.1 Modeling One Tooth Pair

In this section, we model a tooth pair consisting of a pair of open 3D conjugate curves with augmented normals. The tooth pair satisfies the point conjugation conditions listed in Section 4.1 and maintains contact only over a subinterval of the motion period $[0,T)$. By contrast, the conjugate curve pairs realized in [Chen et al. 2024] can be regarded as a special closed-curve realization that maintains contact over the entire period $[0,T)$.

*Modeling a pair of open 3D conjugate curves.* We assume that the driver surface $\mathbf{S}^1$ and the follower surface $\mathbf{S}^2$ have $K$ conjugation points at any $t \in [0,T)$. Following [Chen et al. 2024], each conjugation point is realized by a pair of 3D conjugate curves. Instead of modeling a single pair of closed 3D conjugate curves that keeps contact over $[0,T)$, we model $J$ pairs of open 3D conjugate curves for each conjugation point, each of which keeps contact only over a subinterval of $[0,T)$. We now consider the $j$-th pair of open 3D conjugate curves of the $k$-th conjugation point ($1 \leqslant j \leqslant J$, $1 \leqslant k \leqslant K$), which contacts over a time interval $(t^s_{k,j}, t^e_{k,j})$, where $t^s_{k,j}$ and $t^e_{k,j}$ denote the start and end times of contact; this interval is termed the *contact interval*. During the motions of $\mathbf{S}^1$ and $\mathbf{S}^2$ over $(t^s_{k,j}, t^e_{k,j})$, the $k$-th conjugation point traces a pair of open 3D conjugate curves $\mathbf{p}^\alpha_{k,j}(t)$ on the surfaces $\mathbf{S}^\alpha$, $\alpha \in \{1,2\}$, as well as a locus curve $\mathbf{p}_{k,j}(t)$ in the global frame $\Sigma$; see Figure 4. These curves must satisfy the coincident contact point condition in Section 4.1 for any $t \in (t^s_{k,j}, t^e_{k,j})$:

$$\mathbf{M}^1(t)\mathbf{p}^1_{k,j}(t) = \mathbf{p}_{k,j}(t) = \mathbf{M}^2(t)\mathbf{p}^2_{k,j}(t). \tag{5}$$

Different from [Chen et al. 2024], which parameterizes $\mathbf{p}^2_{k,j}(t)$, we parameterize the locus curve $\mathbf{p}_{k,j}(t)$ as an open 3D cubic B-spline with $l$ control points, denoted by $\{\mathbf{e}_{\mathbf{p}_{k,j}}\}$, to better preserve curve simplicity during optimization. In our experiments, $l = 4$. The pair of open 3D conjugate curves $\mathbf{p}^\alpha_{k,j}(t)$ is then derived as polylines from Equation (5) using $\mathbf{p}_{k,j}(t)$ and the known $\mathbf{M}^\alpha(t)$, $\alpha \in \{1,2\}$.

*Modeling the augmented normals.* Each point on the open 3D conjugate curves $\mathbf{p}^\alpha_{k,j}(t)$ is assigned a unit normal $\mathbf{n}^\alpha_{k,j}(t)$, $\alpha \in \{1,2\}$. According to the coincident normal condition in Section 4.1, the normals satisfy the following relationship (see Figure 4):

$$-\mathbf{M}^1(t)\mathbf{n}^1_{k,j}(t) = \mathbf{n}_{k,j}(t) = \mathbf{M}^2(t)\mathbf{n}^2_{k,j}(t), \tag{6}$$

where $\mathbf{n}_{k,j}(t)$ denotes the *contact normal* at the conjugation point $\mathbf{p}_{k,j}(t)$, $t \in (t^s_{k,j}, t^e_{k,j})$. We follow the approach in [Chen et al. 2024] to model $\mathbf{n}_{k,j}(t)$, which is required to satisfy $\mathbf{n}_{k,j}(t) \cdot \mathbf{T}^\alpha_{k,j}(t) = 0$, $\alpha \in \{1,2\}$, where $\mathbf{T}^\alpha_{k,j}(t) = \mathbf{M}^\alpha(t)\,\dot{\mathbf{p}}^\alpha_{k,j}(t)$ denotes the tangent vector of $\mathbf{p}^\alpha_{k,j}(t)$ at the conjugation point $\mathbf{p}_{k,j}(t)$. We establish a 2D frame $\{\mathbf{N}^2_{k,j}(t), \mathbf{B}^2_{k,j}(t)\}$ in the plane perpendicular to $\mathbf{T}^2_{k,j}(t)$, and express $\mathbf{n}_{k,j}(t)$ as $\mathbf{N}^2_{k,j}(t)\cos\theta_{k,j}(t) + \mathbf{B}^2_{k,j}(t)\sin\theta_{k,j}(t)$, where $\theta_{k,j}(t)$ is modeled by a 1D open cubic B-spline with $\rho$ control points $\{\mathbf{e}_{\theta_{k,j}}\}$, and $\rho = 4$ in our experiments. We enforce $\mathbf{n}_{k,j}(t) \perp \mathbf{T}^1_{k,j}(t)$ by minimizing an energy term $E_{\text{norm}}$. Once $\mathbf{n}_{k,j}(t)$ is obtained, $\mathbf{n}^\alpha_{k,j}(t)$, $\alpha \in \{1,2\}$ follow from Equation (6).

We model a tooth pair, consisting of a pair of open 3D conjugate curves $\mathbf{p}^\alpha_{k,j}(t)$ and the augmented normals $\mathbf{n}^\alpha_{k,j}(t)$, by optimizing the control points $\{\mathbf{e}_{\mathbf{p}_{k,j}}\}$ and $\{\mathbf{e}_{\theta_{k,j}}\}$ to minimize:

$$E_{k,j} = \omega_1 E_{\text{norm}} + \omega_2 E_{\text{tang}} + \omega_3 E_{\text{plan}}, \tag{7}$$

with weights $\omega_1 = 120.0$ and $\omega_2 = \omega_3 = 1.0$. The two additional energy terms are introduced to ensure fabricable geometry. Specifically, $E_{\text{tang}}$ encourages the tangents of the two curves at the conjugation point to be nearly collinear, and $E_{\text{plan}}$ encourages the two curves to be nearly coplanar. The expressions for these energy terms are provided in the supplementary material. The locus curve $\mathbf{p}_{k,j}(t)$ is initialized as a line segment and $\theta_{k,j}(t)$ is initialized to 0.

## 5.2 Modeling $J$ Tooth Pairs as One Sub-Gear Pair

In this section, for a fixed $k$, we model a sub-gear pair using $J$ tooth pairs $\{\{\mathbf{p}^\alpha_{k,j}(t)\}, \{\mathbf{n}^\alpha_{k,j}(t)\}\}$, $\alpha \in \{1,2\}$, $1 \leqslant j \leqslant J$, collectively realizing the $k$-th conjugation point of the conjugate surface pair $\mathbf{S}^1$ and $\mathbf{S}^2$ over the entire interval $[0,T)$. In our experiments, $J = 10$ for each $k$. First, we arrange the contact intervals of the $J$ tooth pairs

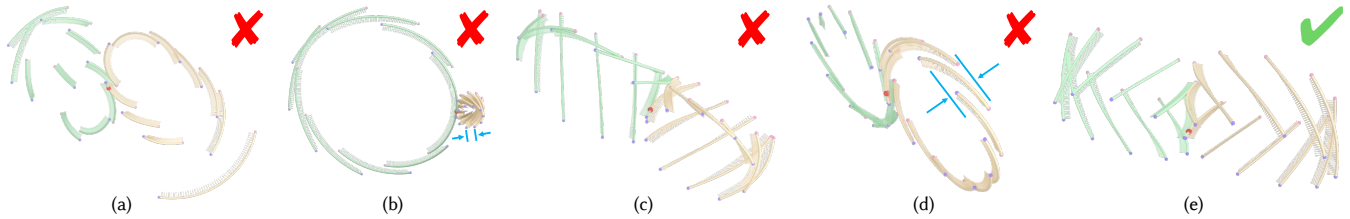


Fig. 6. Modeling the geometry of a sub-gear pair. (a) Without $E_{\text{circ}}$, the start points (purple) and end points (pink) fail to form circular arrangements. (b) Without $C_{\text{spac}}$, consecutive open 3D conjugate curves become too close to each other. (c) Without $E_{\text{para}}$, the circles formed by the start points and end points are not approximately parallel. (d) Without $C_{\text{widt}}$, the two planes containing the circles are too close along the normal direction. (e) A valid sub-gear pair.

to ensure continuous contact throughout $[0, T)$. Second, we introduce additional geometric requirements, leading to a constrained optimization formulation for the sub-gear pair modeling.

*Contact intervals.* As stated in Section 5.1, a single tooth pair maintains contact only within a subinterval $(t^s_{k,j}, t^e_{k,j})$ of $[0, T)$. We do not consider the tooth pair to be in contact at the boundary instants $t^s_{k,j}$ and $t^e_{k,j}$ to prevent contact loss or impact shocks during the transition between consecutive tooth pairs. To ensure that the $J$ tooth pairs maintain continuous contact for any $t \in [0, T)$, their contact intervals must cover the whole period:

$$[0, T) \subset \bigcup_{1 \leqslant j \leqslant J} (t^s_{k,j}, t^e_{k,j}). \tag{8}$$

This equation implies that the contact intervals of consecutive tooth pairs must overlap. To simplify the problem, we uniformly partition the interval $[0, T)$ into $J$ subintervals with $[\tau^s_j, \tau^e_j) = [(j-1)T/J,\ jT/J)$. We then arrange these contact intervals in a traditional gear-like manner:

$$t^s_{k,j} = \tau^s_j - \frac{c-1}{2}\frac{T}{J}, \quad t^e_{k,j} = \tau^e_j + \frac{c-1}{2}\frac{T}{J}, \tag{9}$$

where $c > 1$ denotes the contact ratio in traditional gear design, i.e., the average number of tooth pairs in contact during gear meshing. Times outside $[0, T)$ are interpreted periodically; see Figure 5. In our experiments, $c$ is set to 1.44. Under Equation (9), the $j$-th tooth pair is guaranteed to maintain contact during the $j$-th time interval $[\tau^s_j, \tau^e_j)$. In the remainder of this paper, when computing the measure of dynamic form closure or visualizing contacts of tooth pairs within $[\tau^s_j, \tau^e_j)$, we only consider the $j$-th tooth pair. The remaining portions of $(t^s_{k,j}, t^e_{k,j})$ serve to ensure smooth transitions between consecutive tooth pairs.

*Optimization-based modeling.* Besides the requirements for the contact intervals of the $J$ tooth pairs, these tooth pairs should also be arranged without interference to facilitate fabrication. Two additional energy terms and two constraints are introduced: the energy $E_{\text{circ}}$ encourages the start points (and end points) of each $\mathbf{p}^\alpha_{k,j}(t)$ to form compact, circular arrangements like those in a traditional gear; the constraint $C_{\text{spac}}$ ensures sufficient spacing between consecutive open 3D conjugate curves on the follower surface as well as the driver surface; the energy $E_{\text{para}}$ encourages the circles formed by the start points and the end points to be nearly parallel; and the constraint $C_{\text{widt}}$ guarantees separation along the normal direction of the planes containing the two circles; see Figure 6(a-d) for counter examples. Their formulations are provided in the supplementary material.

Combining Equation (7), we propose a constrained optimization problem to model a sub-gear pair composed of $J$ tooth pairs:

$$\begin{aligned} \min_{\mathcal{P}_k, \vartheta_k} \quad & E_k = \sum_{1 \leqslant j \leqslant J} E_{k,j} + \omega_4 E_{\text{circ}} + \omega_5 E_{\text{para}}, \\ \text{s.t.} \quad & C_{\text{spac}} \leqslant 0, \quad \forall \alpha \in \{1, 2\},\ 1 \leqslant j \leqslant J,\ \chi \in \{s, e\}, \\ & C_{\text{widt}} \leqslant 0, \end{aligned} \tag{10}$$

where $\mathcal{P}_k = \{\{\mathbf{e}_{\mathbf{p}_{k,j}}\}\}_{1 \leqslant j \leqslant J}$ and $\vartheta_k = \{\{\mathbf{e}_{\theta_{k,j}}\}\}_{1 \leqslant j \leqslant J}$ are the geometric parameters and normal parameters of the $J$ tooth pairs. We set $\omega_4 = \omega_5 = 1.0$ in our experiments. The problem is solved using SLSQP [Kraft 1988] implemented in the NLopt package [Johnson 2020]; see Figure 6(e) for a valid result.

## 5.3 Modeling $K$ Sub-Gear Pairs

In this section, we model $K$ sub-gear pairs $\{\{\mathbf{p}^\alpha_{k,j}(t)\}, \{\mathbf{n}^\alpha_{k,j}(t)\}\}$, $\alpha \in \{1, 2\}$, $1 \leqslant j \leqslant J$, $1 \leqslant k \leqslant K$, which are used for modeling all the teeth on the gears; see Figure 7(b). The $K$ sub-gear pairs are required to satisfy the dynamic form closure condition for continuous motion transmission and remain interference-free to ensure fabricability. Following [Chen et al. 2024], we formulate this problem as an optimization problem in Section 5.3.1 and present the solver in Section 5.3.2. To obtain geometry with a favorable load-bearing performance, we use the measure in Section 4.2 to guide the formulation of the objective functions in our optimization.

### 5.3.1 *Optimization Formulation.*

We formulate the modeling of $K$ sub-gear pairs for our mpcGear as an optimization problem, including the search space, objective functions and constraints.

*Search space.* The search space is defined by all the control points of the open 3D conjugate curves $\{\mathcal{P}_k\}_{1 \leqslant k \leqslant K}$ with the augmented normals $\{\vartheta_k\}_{1 \leqslant k \leqslant K}$, and the number of the sub-gear pairs $K$.

*Objective functions.* As discussed in Section 4.2, we require $Q(t) > 0, \forall t \in [0, T)$ for the $K$ sub-gear pairs to satisfy the dynamic form closure condition. We define an indicator function $E_{\text{indi}}(t) = 1$ if $Q(t) > \varepsilon$ and 0 otherwise, with $\varepsilon$ a small positive threshold (set to 0.02 in our experiments). Following the assumption made in Section 5.2, within the $j$-th subinterval $[\tau^s_j, \tau^e_j)$, we consider only the contribution of the $j$-th tooth pair from each sub-gear pair to the dynamic form closure. Thus we introduce the first objective function, which measures the proportion of the motion period $T$

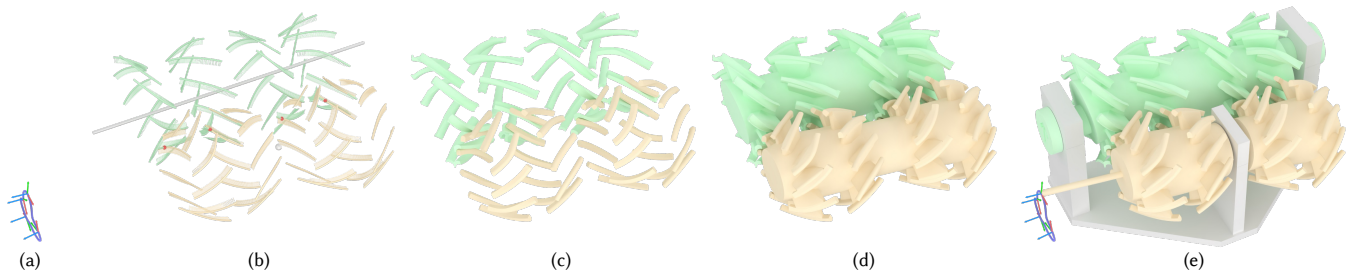


Fig. 7. Modeling a multi-point conjugation gear mechanism. (a) Given the user-specified motion $\mathbf{M}^2(t)$, (b) we first model $K$ sub-gear pairs that satisfy the dynamic form closure condition. (c) Then we model a multi-point conjugation joint by choosing a pair of fixed cross sections to sweep along the optimized 3D conjugate curves to form the surfaces of the teeth. (d) Next, we add spokes and a central hub to connect all the teeth for each gear. (e) Finally, we model the support, the driver-support joint, and the follower-support joint.

over which the dynamic form closure condition is satisfied:

$$E_{\text{validTime}} = \frac{1}{JR} \sum_{1 \leqslant j \leqslant J} \sum_{0 \leqslant r < R} E_{\text{indi}}(t_{j,r}), \tag{11}$$

over $R$ uniform samples $t_{j,r} = (1 - r/R)\,\tau_j^s + (r/R)\,\tau_j^e$, $0 \leqslant r < R$. $R = 36$ in our experiments. The dynamic form closure condition is satisfied when $E_{\text{validTime}} = 1$. In addition, as discussed in Section 4.2, we maximize $Q(t)$ for the $K$ sub-gear pairs to characterize and guide favorable load-bearing performance of the gears. To this end, we introduce the second objective function to evaluate the minimum value of $Q(t)$ throughout $[0, T)$:

$$E_{\text{minMsr}} = \min_{j,r} Q(t_{j,r}). \tag{12}$$

*Constraints.* Our optimization has two constraints. $C_{\text{closure}}$ enforces Equation (3) to exclude the degenerate case. $C_{\text{collision}}$ prevents collisions among the $K$ sub-gear pairs. Please refer to the supplementary material for their expressions.

*5.3.2 Optimization Solver.* For a given $K$, we adopt a two-stage approach to solve for $\{\mathcal{P}_k\}_{1 \leqslant k \leqslant K}$ and $\{\vartheta_k\}_{1 \leqslant k \leqslant K}$. First, multiple candidates are generated by solving the optimization in Equation (10) incorporating the two constraints $C_{\text{closure}}$ and $C_{\text{collision}}$ and an extra energy term $E_{\text{vary}}$ to promote diversity. Then, a genetic algorithm is employed to select and combine candidates to maximize the objective functions in Equations (11) and (12).

According to Equation (2), at least $N + 1$ sub-gear pairs are required to realize an $N$-DOF motion. To obtain a compact mechanism, we start with $K = N + 1$ and attempt to find a solution using the above two-stage approach, and increase $K$ by 1 until we find a feasible solution satisfying the dynamic form closure condition. Implementation details are provided in the supplementary material.

## 5.4 Finalizing the mpcGear Modeling

After optimization, we construct the geometry of a mpcGear by first computing the tooth pairs $\{\{\mathbf{p}_{k,j}^{\alpha}(t)\}, \{\mathbf{n}_{k,j}^{\alpha}(t)\}\}$ from the optimized control points $\{\{\mathcal{P}_k\}, \{\vartheta_k\}\}$ through Equations (5) and (6); see Figure 7(b). Next, we use them to model a multi-point conjugation joint composed of multiple gear teeth modeled by swept surfaces; see Figure 7(c). For both gears, we connect the teeth of each gear into a single rigid body by adding a central hub and a set of spokes that connect the teeth to the hub; see Figure 7(d) and Figure 8(a). Finally, we add the driver-support joint, follower-support joint, and a support, resulting in a complete, fabricable mpcGear; see Figure 7(e). Please refer to the supplementary material for details.

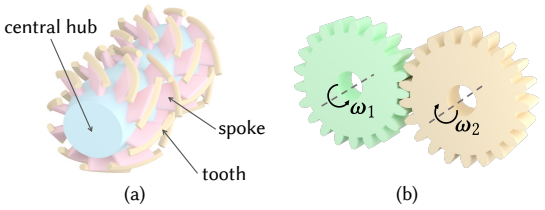


Fig. 8. (a) A gear in a mpcGear with a central hub, multiple teeth, and spokes that connect the teeth to the central hub. (b) A pair of involute gears transferring a 1-DOF rotation to another 1-DOF rotation.

## 6 Results

We implement our approach in C++ and libigl [Jacobson et al. 2018] on a MacBook with a 3.2GHz CPU and 16GB memory. We show that our approach can model mpcGears of different classes (Figure 9), evaluate the kinematic performance of a mpcGear (Figure 10), compare the load-bearing performance of a mpcGear with that of a mpcMech (Figures 11 and 12), and show the practical value of our mpcGears with two applications (Figures 1 and 13). Please refer to the accompanying video for demos. In the supplementary material, we present a table providing statistics of all results shown in this paper. Overall, modeling a mpcGear takes from 16 to 147 minutes. Lower DOFs of the motion space typically result in shorter times.

*Modeling various classes of mpcGears.* We present four classes of mpcGears, including mpcGear_1R, mpcGear_1R1T, mpcGear_3R and mpcGear_3R1T; see Figure 9. We find that the required number of sub-gear pairs $K$ increases with the DOFs of the motion space, which is consistent with [Chen et al. 2024]. However, for the same motion space, our mpcGears require a smaller $K$ than mpcMechs. In the first three results, $K$ reaches its minimum theoretical value $N + 1$ given by Equation (2). We reasonably attribute this to the use of more flexible, freeform *open* 3D conjugate curves in our modeling, which enables dynamic form closure to be satisfied with fewer contacts, as opposed to *closed* curves.

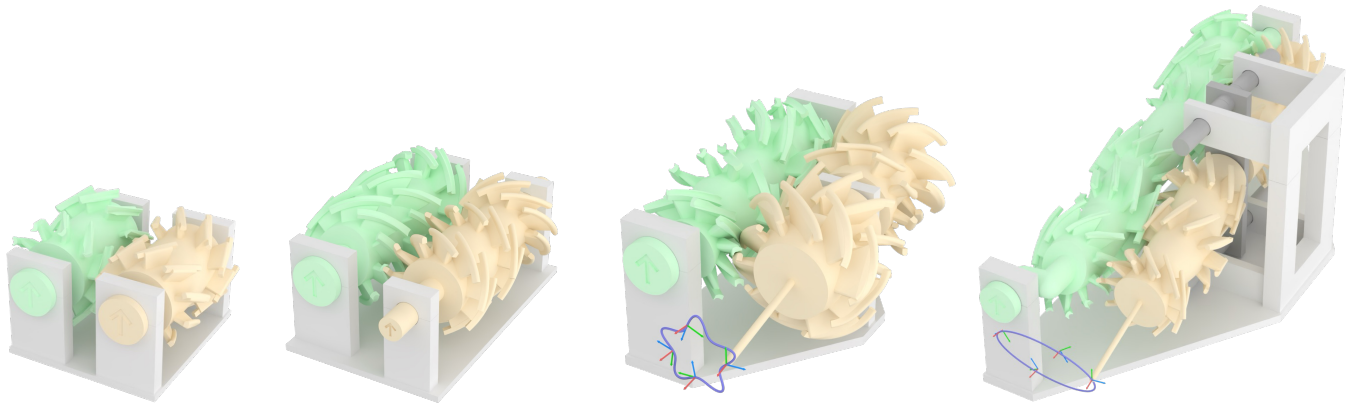

(a) mpcGear_1R (b) mpcGear_1R1T (c) mpcGear_3R (d) mpcGear_3R1T

Fig. 9. Four classes of mpcGears that we have modeled, where the follower gear (yellow) can perform (a) 1-DOF rotation, (b) 1-DOF rotation and 1-DOF translation, (c) 3-DOF rotation, and (d) 3-DOF rotation and 1-DOF translation.

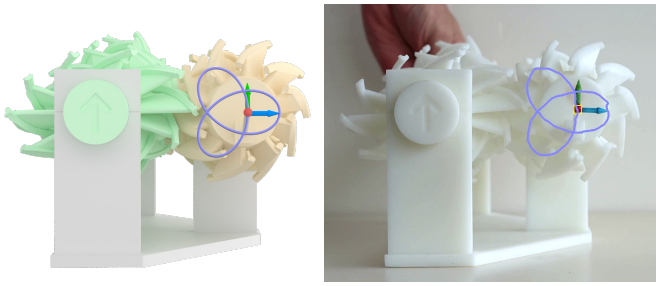

Fig. 10. Evaluating the kinematic performance of a mpcGear_3R for generating a 3D motion, where the end-effector traces a Trefoil curve. (Left) Our modeled mpcGear_3R. (Right) The 3D printed prototype, where the generated trajectory is tracked in video frames and visualized in purple.

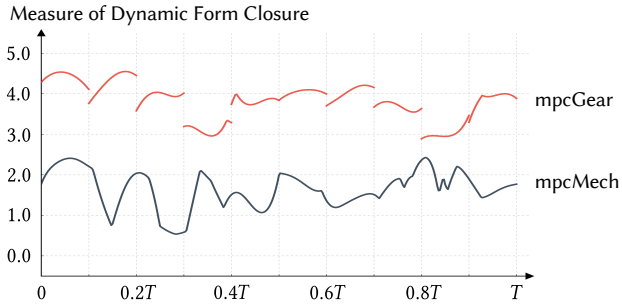


Fig. 11. Comparison of the measure of dynamic form closure between mpcMech (black) and our mpcGear (red) over a full motion period $[0, T)$.

We also briefly compare mpcGears with traditional gear pairs. Traditional gear pairs are more compact, structurally simpler, and likely more efficient for transferring motions in a low-DOF motion space, typically rotary motion transmission between two shafts; see Figure 8(b) for an involute gear pair. In contrast, the mpcGear_1R in Figure 9(a) is less compact and more complex because it contains two sub-gear pairs. However, our mpcGears can generate motions in high-DOF motion spaces that traditional gear pairs cannot directly realize; see Figure 9(c-d).

*Evaluation of kinematic performance.* To evaluate the kinematic performance of mpcGears, we model and fabricate a mpcGear_3R to generate a specified motion; see Figure 10. The motion follows a Trefoil curve on a spherical surface with simultaneous rotation. We visualize the motion by attaching a red sphere and two arrows to the end-effector. The mechanism is fabricated using SLA 3D printing with a resolution of 0.1 mm. We track the path generated by the red sphere using an image-based approach. Figure 10 compares the virtual result and the 3D printed prototype from the front view. The result shows that our mpcGear functions well as a working mechanism, with the driver gear continuously transferring motion to the follower gear, as enabled by satisfying the dynamic form closure condition. Moreover, both the tracked trajectory and arrow directions closely match their virtual counterparts throughout the motion. Please refer to the accompanying video. The discrepancy between the trajectories may be caused by fabrication tolerances and material deformation, which can be reduced by more precise manufacturing and tougher materials.

*Comparison with mpcMech.* We evaluate load-bearing performance by comparing mpcGears with mpcMechs [Chen et al. 2024]. First, we model a mpcGear_3R and a mpcMech_3R for the same 3-DOF rotation, optimize both mechanisms using the measure in Equation (4), and use identical support geometry in both designs; see rows 1-2 of Figure 12. We compute the measure value for both mechanisms over $t \in [0, T)$; see Figure 11. Our mpcGear consistently maintains a higher measure than the mpcMech, with improvements ranging from 20.9% to 633.2% over $[0, T)$. Second, for further verification, we fabricate 3D printed prototypes of both mechanisms; see rows 3-6 of Figure 12 and the accompanying video. Both mechanisms are fixed to a table, and a grooved cylindrical component is attached to the follower at the same location, with a rope and a 10g slotted weight hanger. Each follower's center of mass is aligned with the ball joint

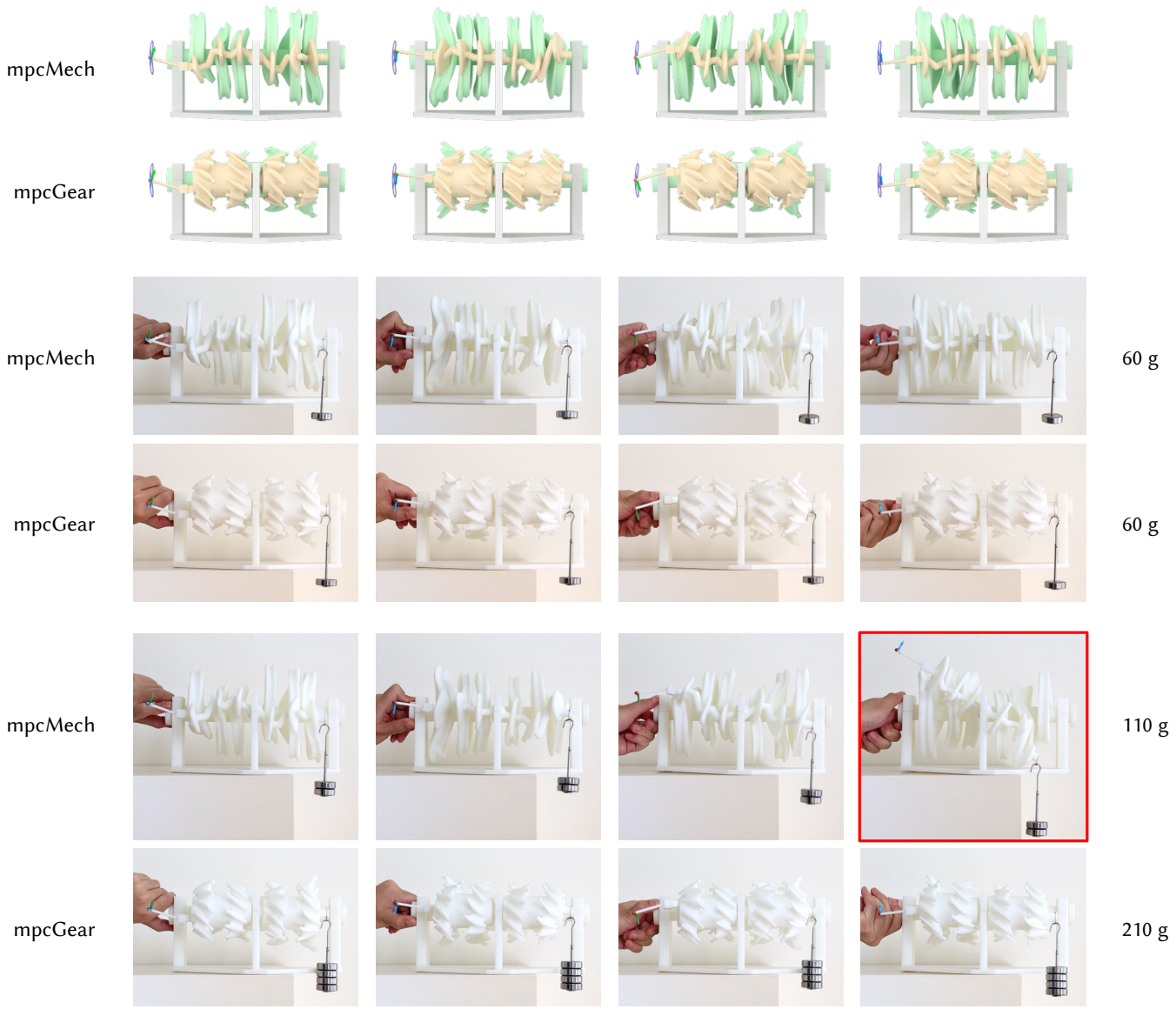


Fig. 12. Comparison of load-bearing performance between mpcMech and mpcGear through a physical experiment. (Rows 1-2) Four key poses of mpcMech_3R and mpcGear_3R generating the same motion, where the leftmost column shows the first key pose. (Rows 3-4) mpcMech_3R and mpcGear_3R both carrying a 60g load. (Rows 5-6) mpcMech_3R carrying a 110g load and mpcGear_3R carrying a 210g load.

to eliminate gravity-induced moments. We examine whether each mechanism can still generate the prescribed motion under increasing weights. Both mechanisms complete the full motion under a 60g load, but the mpcMech loses contact at the fourth pose under a 110g load, whereas our mpcGear still completes the motion under a 210g load. In our experiments, the mpcMech is able to complete the motion under loads up to 100g, so the resulting improvement of at least 110% is consistent with the difference predicted by Figure 11, noting that the measure evaluates the worst-case effective wrench (torque in mpcGear_3R) over all directions in $U$, while this experiment considers only the direction of the torque produced by the gravity of the weights. These results suggest that mpcGears modeled using open 3D conjugate curves exhibit improved load-bearing performance compared to mpcMechs modeled by closed 3D conjugate curves.

*Applications.* We showcase the practical value of our mpcGears using two applications. First, we model and fabricate a mpcGear_3R to realize a low-cost manipulator that is driven by a single actuator and capable of performing a load-bearing pick-and-place task; see Figure 1. The follower gear lifts and transfers a tray loaded with four 200g weights (800g total), performing a complex 3-DOF rotational

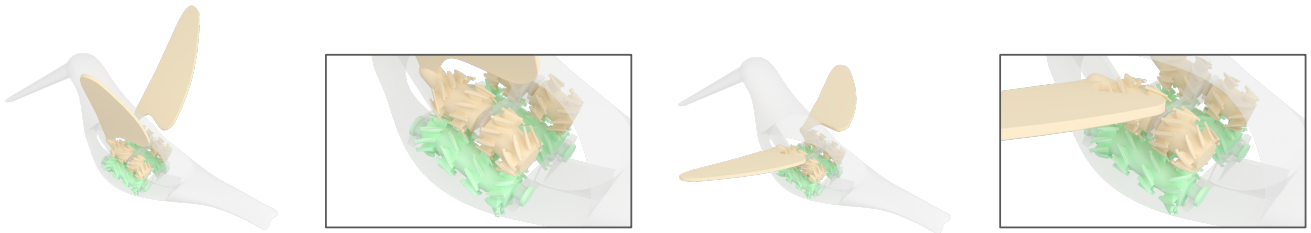


Fig. 13. A flapping wing mechanism modeled using mpcGears to perform bird-like flapping motions. (a) and (c) show two key poses of the mechanism, while (b) and (d) provide corresponding close-up views highlighting the details of the mpcGears.

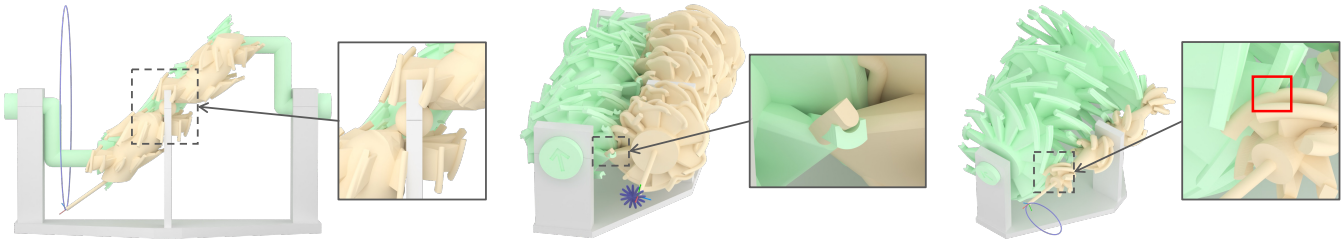


Fig. 14. Three representative failure cases. (a) A target motion with an overly large range causes the follower gear to overlap with the support region. (b) A target motion whose end-effector trajectory contains too many high-curvature points causes a follower tooth to overlap with a driver tooth and its spoke. (c) When the driver gear has 12 teeth and the follower gear has 6 teeth, a driver tooth collides with a non-corresponding follower tooth.

motion in which the tray continuously changes its orientation during manipulation. Second, we apply mpcGears to a flapping-wing mechanism, where a pair of mpcGear_3Rs generates symmetric motions; see Figure 13. The reciprocating rotations of the driving gears generate 3-DOF flapping motions, suggesting the potential of mpcGears for applications involving aerodynamic loads.

*Limitations.* One strength of our mpcGears is their ability to exactly generate a user-specified motion. However, this does not mean that our approach can model a mpcGear for arbitrary motions, and the design space is still not fully understood mainly because of fabrication constraints. Figure 14 shows three representative failure cases caused by unfabricable geometries: a target motion with an overly large range may make it infeasible to add the support because the follower gear may overlap with the support region; an end-effector trajectory with high-curvature points may cause twisted follower teeth, leading to tooth collisions; and when the driver has more teeth than the follower, the resulting driver teeth may become overly long and collide with non-corresponding follower teeth. A detailed discussion of the effects of unequal tooth numbers is provided in the supplemental material.

## 7 Conclusion

We present a new class of unconventional gear mechanisms called multi-point conjugation gear mechanisms (mpcGears), in which the driver gear can transfer motion to the follower gear continuously via multiple conjugation points. Our work models mpcGears for 3D motion generation under external loads based on gear geometry with multi-point conjugation. We introduce an optimization-based approach to model mpcGears, in which the dynamic form closure condition is satisfied to ensure continuous motion transmission, while the measure of dynamic form closure is used to evaluate and guide the load-bearing performance induced by the gear geometry. The effectiveness of our approach is demonstrated by the diverse mpcGears we modeled. Our work shows that complex motion information can be successfully encoded into gear geometry.

*Future work.* Several promising directions remain for future work. First, this work mainly focuses on the motion generation ability and load-bearing performance of mpcGears. An important direction is to conduct more comprehensive mechanical analyses, such as analyses of contact stress, transmission efficiency, and sensitivity to tolerances. Second, another direction is to explore mechanical systems composed of multiple mpcGears to enable coordinated or multiple output motions, analogous to conventional gear trains. Finally, we plan to combine mpcGears with other mechanical components, such as cams, linkages, and belts, to enable more applications in engineering and robotics.

## Acknowledgments

We thank the reviewers for their valuable comments. This work was supported by the Singapore MOE AcRF Tier 2 Grant (MOE-T2EP20222-0008), the Singapore MOE AcRF Tier 1 Grant (RG107/25), the Laoshan Laboratory (No. LSKJ202300305), and the National Natural Science Foundation of China (62025207).

## References


Kazuki Abe, Kenjiro Tadakuma, and Riichiro Tadakuma. 2021. ABENICS: Active Ball Joint Mechanism with Three-DoF Based on Spherical Gear Meshings. *IEEE Transactions on Robotics* 37, 5 (2021), 1806–1825.

Gaurav Bharaj, Stelian Coros, Bernhard Thomaszewski, James Tompkin, Bernd Bickel, and Hanspeter Pfister. 2015. Computational Design of Walking Automata. In *Proc. ACM SIGGRAPH/Eurographics Symp. on Computer Animation*. 93–100.

Duygu Ceylan, Wilmot Li, Niloy J. Mitra, Maneesh Agrawala, and Mark Pauly. 2013. Designing and Fabricating Mechanical Automata from Mocap Sequences. *ACM Trans. on Graph. (SIGGRAPH Asia)* 32, 6 (2013), 186:1–186:11.

Bingkui Chen, Dong Liang, and Yane Gao. 2014a. Geometry Design and Mathematical Model of a New Kind of Gear Transmission with Circular Arc Tooth Profiles Based on Curve Contact Analysis. *Proceedings of the Institution of Mechanical Engineers, Part C: Journal of Mechanical Engineering Science* 228, 17 (2014), 3200–3208.

Bingkui Chen, Dong Liang, and Zhaoyang Li. 2014b. A Study on Geometry Design of Spiral Bevel Gears Based on Conjugate Curves. *International Journal of Precision Engineering and Manufacturing* 15, 3 (2014), 477–482.

Chih-Hsin Chen. 1978. On Theory of Conjugate Surfaces. In *Proc. the World Symposium on Gears and Transmissions*, Vol. A. 119–132.

Ke Chen, Siqi Li, Peng Song, Jianmin Zheng, and Ligang Liu. 2024. mpcMech: Multi-Point Conjugation Mechanisms. *ACM Trans. on Graph. (SIGGRAPH Asia)* 43, 6 (2024), 211:1–211:14.

Yingjie Cheng, Peng Song, Yukun Lu, Wen Jie Jeremy Chew, and Ligang Liu. 2022. Exact 3D Path Generation via 3D Cam-Linkage Mechanisms. *ACM Trans. on Graph. (SIGGRAPH Asia)* 41, 6 (2022), 225:1–225:13.

Yingjie Cheng, Yucheng Sun, Peng Song, and Ligang Liu. 2021. Spatial-Temporal Motion Control via Composite Cam-follower Mechanisms. *ACM Trans. on Graph. (SIGGRAPH Asia)* 40, 6 (2021), 270:1–270:15.

Vincent Commin, Samuel Peltier, Arthur Cavalier, and Sébastien Horna. 2025. Clock mechanism generation using interaction graphs. *Comp. & Graph.* 132 (2025), 104317:1–104317:9.

Jordi Cornellà and Raúl Suárez. 2009. Efficient Determination of Four-point Form-closure Optimal Constraints of Polygonal Objects. *IEEE Transactions on Automation Science and Engineering* 6, 1 (2009), 121–130.

Stelian Coros, Bernhard Thomaszewski, Gioacchino Noris, Shinjiro Sueda, Moira Forberg, Robert W. Sumner, Wojciech Matusik, and Bernd Bickel. 2013. Computational Design of Mechanical Characters. *ACM Trans. on Graph. (SIGGRAPH)* 32, 4 (2013), 83:1–83:12.

Kapil Gupta, Neelesh Kumar Jain, and Rudolph Laubscher. 2017. *Advanced Gear Manufacturing and Finishing: Classical and Modern Processes.* Academic Press.

Yujie Hou and Chao Lin. 2020. Kinematic Analysis and Experimental Verification of An Oval Noncircular Bevel Gears with Rotational and Axial Translational Motions. *Journal of the Brazilian Society of Mechanical Sciences and Engineering* 42, 1 (2020), 60:1–60:11.

Yanan Hu, Chao Lin, Shuo Li, Yongquan Yu, Chunjiang He, and Zhiqin Cai. 2021. The Mathematical Model of Curve-Face Gear and Time-Varying Meshing Characteristics of Compound Transmission. *Applied Sciences* 11, 18 (2021), 8706:1–8706:26.

Alec Jacobson, Daniele Panozzo, et al. 2018. libigl: A simple C++ geometry processing library. https://libigl.github.io/.

Steven G. Johnson. 2020. The NLopt nonlinear-optimization package. http://github.com/stevengj/nlopt.

Dieter Kraft. 1988. A Software Package for Sequential Quadratic Programming. *DLR German Aerospace Center-Institute for Flight Mechanics* (1988).

Kannan Lakshminarayan. 1978. *Mechanics of Form Closure.* Technical Report. Indian Institute of Technology Madras. 2–8 pages.

Siqi Li, Haoyu Tang, Peng Song, Bailin Deng, and Jianmin Zheng. 2025. Conformable mechanisms on freeform surfaces. *Comp. & Graph.* 132 (2025), 104359:1–104359:13.

Faydor L. Litvin, Alfonso Fuentes-Aznar, Ignacio Gonzalez-Perez, and Kenichi Hayasaka. 2009. *Noncircular Gears: Design and Generation.* Cambridge University Press.

Yang Liu and J. Michael McCarthy. 2017. Design of a Linkage System to Write in Cursive. *Journal of Computing and Information Science in Engineering* 17, 3 (2017), 031015:1–031015:8.

Gang Lv, Shouwen Fan, and Xin Zhang. 2016. Study on The Design and The Shaping of The Pitch Surface of A Multi-lobed Non-circular Bevel Gear. *Proceedings of the Institution of Mechanical Engineers, Part D: Journal of Automobile Engineering* 230, 4 (2016), 542–553.

Guirec Maloisel, Christian Schumacher, Espen Knoop, Ruben Grandia, and Moritz Bächer. 2023. Optimal Design of Robotic Character Kinematics. *ACM Trans. on Graph.* 42, 6 (2023), 195:1–195:15.

Dominik Mannhart, Fabio Dubois, Karen Bodie, Victor Klemm, Alessandro Morra, and Marco Hutter. 2020. CAMI - Analysis, Design and Realization of a Force-Compliant Variable Cam System. In *Proc. IEEE Int. Conf. on Robotics and Automation*. 850–856.

Elisabetta A Matsumoto and Henry Segerman. 2023. A mathematical overview and some applications of gear design. *3D Printing in Mathematics* 79 (2023), 1–17.

Vittorio Megaro, Bernhard Thomaszewski, Damien Gauge, Eitan Grinspun, Stelian Coros, and Markus Gross. 2014. ChaCra: An Interactive Design System for Rapid Character Crafting. In *Proc. ACM SIGGRAPH/Eurographics Symp. on Computer Animation*. 123–130.

G. Nishida, A. Bousseau, and D. G. Aliaga. 2019. Multi-Pose Interactive Linkage Design. *Comp. Graph. Forum (Eurographics)* 38, 2 (2019), 277–289.

Hyunjoo Oh, Jeeeun Kim, Cory Morales, Mark Gross, Michael Eisenberg, and Sherry Hsi. 2017. FoldMecha: Exploratory Design and Engineering of Mechanical Papercraft. In *Proceedings of the Eleventh International Conference on Tangible, Embedded, and Embodied Interaction*. 131—-139.

Robin Roussel, Marie-Paule Cani, Jean-Claude Léon, and Niloy J. Mitra. 2018. Exploratory Design of Mechanical Devices with Motion Constraints. *Comp. & Graph. (Computational Fabrication)* 74 (2018), 244–256.

Peng Song, Xiaofei Wang, Xiao Tang, Chi-Wing Fu, Hongfei Xu, Ligang Liu, and Niloy J. Mitra. 2017. Computational Design of Wind-up Toys. *ACM Trans. on Graph. (SIGGRAPH Asia)* 36, 6 (2017), 238:1–238:13.

Takuto Takahashi and Hiroshi G. Okuno. 2018. Design and Implementation of Programmable Drawing Automata based on Cam Mechanisms for Representing Spatial Trajectory. In *Proc. IEEE/RSJ Intl. Conf. on Intelligent Robots and Systems*. 450–455.

Bernhard Thomaszewski, Stelian Coros, Damien Gauge, Vittorio Megaro, Eitan Grinspun, and Markus Gross. 2014. Computational Design of Linkage-Based Characters. *ACM Trans. on Graph. (SIGGRAPH)* 33, 4 (2014), 64:1–64:9.

Oskar van Deventer. 2019. That Is Not Art, It Is a Puzzle!. In *Proc. Bridges: Mathematics, Music, Art, Architecture, Culture*. 1–8.

Daren Wu and Jiashun Luo. 1992. *A Geometric Theory of Conjugate Tooth Surfaces.* World Scientific Publishing Company.

Hao Xu, Tianwen Fu, Peng Song, Mingjun Zhou, Chi-Wing Fu, and Niloy J. Mitra. 2020. Computational Design and Optimization of Non-Circular Gears. *Comp. Graph. Forum (Eurographics)* 39, 2 (2020), 399–409.

Hongyi Xu, Espen Knoop, Stelian Coros, and Moritz Bächer. 2018. Bend-It: Design and Fabrication of Kinetic Wire Characters. *ACM Trans. on Graph. (SIGGRAPH Asia)* 37, 6 (2018), 239:1–239:15.

Bowen Yu and Kwun-Lon Ting. 2011. Free-Form Conjugation Theory. In *Proceedings of the ASME International Design Engineering Technical Conferences and Computers and Information in Engineering Conference*, Vol. 6. 481–492.

Bowen Yu and Kwun-Lon Ting. 2013a. Free-Form Conjugation Modeling and Gear Tooth Profile Design. *Journal of Mechanisms and Robotics* 5, 1 (2013), 011001:1–011001:9.

Bowen Yu and Kwun-Lon Ting. 2013b. Manifold Conjugation and Discrete Gear Design. In *Proceedings of the ASME International Design Engineering Technical Conferences and Computers and Information in Engineering Conference*, Vol. 5. V005T11A028:1–V005T11A028:10.

Lu-he Zhang, Shi-xuan Li, Jian Huang, and Bing-kui Chen. 2019. Theoretical and Experimental Investigations of Gear Transmission with Geometric Elements Constructed Tooth Pairs Having Triple Contact Points. *International Journal of Precision Engineering and Manufacturing* 20 (2019), 1197–1206.

Fangyan Zheng, Lin Hua, Xinghui Han, and Dingfang Chen. 2016. Generation of Noncircular Bevel Gears with Free-Form Tooth Profile and Curvilinear Tooth Lengthwise. *Journal of Mechanical Design* 138, 6 (2016), 064501:1–064501:7.

Lifeng Zhu, Weiwei Xu, John Snyder, Yang Liu, Guoping Wang, and Baining Guo. 2012. Motion-Guided Mechanical Toy Modeling. *ACM Trans. on Graph. (SIGGRAPH Asia)* 31, 6 (2012), 127:1–127:10.